

Proton and Pion Production in Au+Au Collisions at 10.8A

GeV/c

J. Barrette⁵, R. Bellwied⁹, S. Bennett⁹, R. Bersch⁷, P. Braun-Munzinger², W. C. Chang⁷,
W. E. Cleland⁶, M. Clemen⁶, J. Cole⁴, T. M. Cormier⁹, Y. Dai⁵, G. David¹, J. Dee⁷,
O. Dietzsch⁸, M. Drigert⁴, K. Filimonov³, S. C. Johnson⁷, J. R. Hall⁹, T. K. Hemmick⁷,
N. Herrmann², B. Hong², Y. Kwon⁷, R. Lacasse⁵, Q. Li⁹, T. W. Ludlam¹, S. K. Mark⁵,
R. Matheus⁹, S. McCorkle¹, J. T. Murgatroyd⁹, D. Miśkowiec², E. O'Brien¹, S. Panitkin⁷,
P. Paul⁷, T. Piazza⁷, M. Pollack⁷, C. Pruneau⁹, Y. J. Qi⁵, M. N. Rao⁷, E. Reber⁴,
M. Rosati⁵, N. C. daSilva⁸, S. Sedykh⁷, U. Sonnadara⁶, J. Stachel³, E. M. Takagui⁸, V.
Topor Pop⁵, S. Voloshin⁶, T. B. Vongpaseuth⁷, G. Wang⁵, J. P. Wessels³, C. L. Woody¹,
N. Xu⁷, Y. Zhang⁷, C. Zou⁷

(E877 Collaboration)

¹ *Brookhaven National Laboratory, Upton, NY 11973*

² *Gesellschaft für Schwerionenforschung, 64291 Darmstadt, Germany*

³ *Universität Heidelberg, 69120 Heidelberg, Germany*

⁴ *Idaho National Engineering Laboratory, Idaho Falls, ID 83402*

⁵ *McGill University, Montreal, Canada*

⁶ *University of Pittsburgh, Pittsburgh, PA 15260*

⁷ *SUNY, Stony Brook, NY 11794*

⁸ *University of São Paulo, Brazil*

⁹ *Wayne State University, Detroit, MI 48202*

(April 26, 2000)

Abstract

We present proton and pion transverse momentum spectra and rapidity distributions for Au+Au collisions at 10.8A GeV/c. The proton spectra exhibit

collective transverse flow effects. Evidence of the influence of the Coulomb interaction from the fireball is found in the pion transverse momentum spectra. The data are compared with the predictions of the RQMD event generator.
PACS number(s) : 25.75.+r

I. INTRODUCTION

One of the main motivations of the relativistic heavy-ion program is the formation of baryonic matter at extreme temperatures and densities, and the subsequent characterization of such matter. Of central importance is the ability to understand to what extent the nuclear matter has been compressed and heated. At the AGS, Au+Au collisions at about 11A GeV/c have been characterized rather completely in terms of the global observables such as transverse energy [1] and charged particle multiplicity [2]. From these measurements, it was concluded that central Au+Au collisions exhibit a large degree of stopping and leads to larger energy density than lighter systems at the same bombarding energy. Through comparisons with models that reproduce the experimental data, it has been concluded that one reaches baryon densities of up to 10 times normal nuclear matter density and energy densities of the order of 2 GeV/fm³ in the center of the fireball [3]. These are in the range of parameters where based on QCD calculations one expects a baryon-rich deconfined phase. Distributions in rapidity and transverse momentum of the particles emitted in such collisions contain more complete information about the degree of stopping attained and provide more sensitive tests of the validity of the model predictions. Semi-inclusive proton and pion distributions from central Au+Au reactions at 11.6A GeV/c have been reported in Ref [4]. It was observed that the rapidity distribution for protons has a maximum around mid-rapidity consistent with a large degree of stopping and hence high baryon density. In this paper we present measurements of the forward-rapidity inclusive double differential multiplicities and rapidity distributions for proton and pions in central Au+Au collisions at a beam momentum of 10.8A GeV/c.

II. EXPERIMENT

The experiment was performed using the E877 apparatus at the AGS at the Brookhaven National Laboratory. The E877 set-up used in this experiment is an upgrade of the E814

apparatus which has been previously described in Ref. [5]. The device features nearly 4π calorimetry surrounding the target. The information from the calorimeters was used in this work primarily for centrality selection. Charged particles emitted in the forward direction ($-134 \text{ mrad} < \theta_{horizontal} < 16 \text{ mrad}$ and $-11 \text{ mrad} < \theta_{vertical} < 11 \text{ mrad}$) are analyzed by a magnetic spectrometer. The spectrometer has been significantly upgraded so as to handle the high multiplicity of charged particles produced in the Au collisions. Inserted between two high resolution drift chambers are four new multiwire proportional chambers which aid in the pattern recognition by confirming links between the drift chambers. The section of the spectrometer which receives primary beam particles was purposely made insensitive to avoid saturation and failure of the tracking devices. A new 150 slat high-resolution time-of-flight hodoscope [6] was installed downstream of the tracking chambers, 12 meters from the target. The average time resolution of the hodoscope was 85 ps. Particles are identified by measuring their momentum and velocity. The system provides proton-pion separation, at the 2.5σ level, up to a momentum of 8.8 GeV/c. The momentum resolution ($\delta p/p \sim 3\%$) of the tracking system is dominated by multiple scattering. Contamination from high momentum kaons is estimated to contribute less than 5 % to the measured proton yield at all rapidities and to the experimental π^+ yield at rapidities $y < 3.8$. The kaon contamination will increase slowly with rapidity is an estimated to reach up to 10 % of the measured pion yield at $y = 4.4$.

In order to reconstruct the pion and proton spectra, the data must to be corrected for the spectrometer acceptance and the effects of the various conditions introduced in the analysis. The acceptance corrections for the distributions have been calculated using Monte Carlo simulation. The acceptance corrections on the final data sample were calculated as function of rapidity y and transverse momentum p_t by propagating generated particles through the E877 apparatus. All known effects of the spectrometer geometry , detector resolutions, kinematics and cuts were included. For pion spectra the influence of pion decay is included in the program used to calculate the acceptance of the spectrometer.

For central Au+Au collisions the mean spectrometer occupancy is about 7-8 charged par-

ticles per event, and is strongly position dependent in the bending plane of the spectrometer, varying from 1% to 18% per drift chamber sense wire. Track reconstruction efficiency decreases abruptly when two tracks are closer than twice the wire spacing in a drift chamber. The occupancy variation introduces a position dependent efficiency for track reconstruction and is a source of systematic error. Two correction procedures were developed as part of a set of independent data analyses. Each of the procedures used the *measured* occupancy in all tracking devices as its basis, thereby avoiding model dependence in the correction. The first method [7] involved a detailed model of the track reconstruction efficiency as a function of track separation. Each track is given a weight that, to first order, accounts for the tracks that are lost due to the presence of the track seen. No tracks are removed from the data sample in this method. The other method rejected every pair of tracks which in a given detector failed a minimum separation cut below which the tracking efficiency is less than unity [8,9]. In this case the effect of the cut was calculated either by adding virtual tracks to the events and computing the probability that such tracks fail the minimum cut. The correction factor varies from 1.1 to 1.3, the largest correction being for tracks passing near the deadened beam region. The two correction methods give very similar results with maximum differences of 5%. The second correction procedure was also tested in a simulation using the GEANT [10] package. Application of the correction procedure to the Monte Carlo generated data tracked through the spectrometer reproduces the initial distribution with maximum deviations of 5%. Considering the agreement both between the two correction methods and with the GEANT simulation, and the systematic uncertainties in overall single track reconstruction efficiency, we deduce a combined systematic error of less than 10%. All data points in the figures have statistical error bars only, which are often smaller than the data point symbol.

Central collisions were defined as those producing high transverse energy in the pseudo-rapidity interval $-0.5 < \eta < 0.8$, where $\eta = -\ln[\tan(\theta/2)]$, such that $\sigma_{central}$ is 4% of the geometric cross section. The resolution on the centrality has been estimated by studying the fluctuation in the transverse energy (E_t) distribution in the solid angle covered by the

target calorimeter TCAL that is used to determine the collision centrality. This results in a smooth cut-off in the impact parameter distribution that is taken into account in generating the calculated spectra. Based on RQMD simulations it is estimated that the selected events correspond to a mean impact parameter of about 2.4 fm. For the 0 – 4% centrality cut this resolution in impact parameter is estimated to be ≈ 0.7 fm.

III. RESULTS

A. Protons

Fig. 1 shows the measured proton transverse mass spectra for central Au+Au collisions. The vertical axis is $(1/m_t^2) \times (d^2N/dm_t dy)$, the representation in which a Boltzmann (or thermal) distribution is a pure exponential in m_t ($m_t = \sqrt{p_t^2 + m^2}$). The spectra are close to exponential. One notes, however, a steep component at low m_t for rapidities near $y_{beam}=3.14$, which in Si+A collisions was identified as due to the projectile spectator nucleons [11].

Also plotted are the results of two component Boltzmann fits to the data (full lines). The dashed lines near beam rapidity show the contribution from the component with large inverse slope parameter T_B that can be attributed to emission from the central “fireball”. This component always dominates at $m_t - m$ larger than 0.1 GeV/c². The histograms correspond to the prediction of the RQMD event generator [12] (RQMD 1.08).

As it was done for the experimental data, the analysis of the RQMD generated events included selection of the 4% most central collisions from the produced E_t in the pseudo-rapidity interval $-0.5 < \eta < 0.8$. RQMD treats the projectile and target as an unbound ensemble of nucleons with Fermi energy distributions. This introduces a large unphysical excess in the number of calculated spectator nucleons. These were removed by considering in the calculated spectra only protons that have had one or more interactions.

RQMD reproduces quite well the average multiplicities but the calculated spectra are consistently steeper than the data.

The systematic differences between the data and the model predictions are better shown in Fig. 2 where we compare the values of fitted inverse slope parameters T_B as a function of rapidity, with RQMD predictions. At each rapidity the calculated spectra were fitted over the range covered by experimental data.

The rapidity dependences of the measured and predicted inverse slope parameters are very similar but the RQMD spectra give values that are systematically about 20% lower than the data. The derived slope parameters increase very rapidly near central rapidity. This is different than what was observed for Si+Al collisions [5,13] and also deviate from the $1/\cosh(y)$ dependence expected for an isotropically expanding fireball.

The observed behavior can be explained by the presence of strong transverse collective flow in the measured spectra near midrapidity. Transverse collective flow leads to deviation from the exponential shape expected for a pure thermal source [14–16].

In particular, transverse flow results in flatter distribution (i.e. higher value of T_B) at low m_t . This flattening which has been observed [4] is predicted to increase with the flow velocity and with the mass of the produced particles. The fact that the measured spectra are flatter than the calculated spectra suggests that the pure cascade version of RQMD as implemented in RQMD 1.08 predicts a too small collective flow. A similar conclusion has been reached in Ref. [17] from a study of the proton and pion azimuthal distributions measured relative to the reaction plane.

This is also consistent with the results shown in Fig. 3 where we compare the proton spectra predicted by RQMD 2.3 for Au+Au collisions in cascade mode and including the effect of mean field. The introduction of mean-field in RQMD gives somewhat flatter spectra particularly at low value of m_t and close to mid-rapidity.

The predicted effect of the mean field on the deduced inverse slope parameter in our acceptance is shown in Fig. 4. The cascade results are in good agreement with those in Fig. 2 when taken into account the shift $\Delta y = 0.03$ in the center of mass rapidity between the two energies. The introduction of mean field in RQMD 2.3 has little effect on the inverse slope parameter at the most forward rapidities, but give results in much better agreement

with the data closer to midrapidity.

The proton rapidity distribution dN/dy is presented in Fig. 5. It has been obtained by integrating over the transverse mass using the measurements where available and extending the integral analytically to $p_t = 0$ and $p_t \rightarrow \infty$ using the results from the exponential fits. This procedure was tested using the spectra calculated with RQMD. The data points nearest to the center of mass have been omitted since the limited m_t range of the measured spectra results in large systematic errors. It is estimated that the extrapolation leads to an overestimation of the yield for the first data point in Fig. 5 at $y=2.55$ by a maximum of roughly 15 % while the systematic error is negligible for data points at $y \geq 2.85$. The stars represent the contribution to the total proton multiplicity from the low m_t component calculated from the fitted spectra. As expected, it is centered near $y_{beam}=3.14$. It is a relatively small contribution to the total proton multiplicity. The peak near beam rapidity integrates to one proton. In the measured rapidity range, RQMD (histogram) reproduces fairly well the measured rapidity distribution. The calculated distribution shows a weak inflexion near beam rapidity that can be associated with spectator-like protons that have had minimal interaction in the collision.

B. Pions

The transverse mass spectra for π^+ and π^- are presented in Fig. 6. The solid curves show Boltzmann fits to the data. Exponential functions are fitted to the data above to $m_t - m_\pi \geq 175$ MeV/c² in the rapidity bins where available, $y \leq 3.4$ for π^+ and $y \leq 3.9$ for π^- , and starting from $m_t - m_\pi = 0$ GeV/c² at higher rapidities.

As observed for Si+Pb system [18], the spectra show a significant enhancement over a Boltzmann distribution at low m_t . This has been attributed to the contribution from the decay of Δ resonances and higher mass resonances [18–21]. The rapidity dependence of the shape of the spectra and the magnitude of low p_t enhancement attributed to resonance decay pions are well reproduced by RQMD. The calculation slightly over-estimates the yield

of negative pions especially at high rapidities.

The pion rapidity distributions for π^+ and π^- are obtained by integrating over the transverse mass, using the measured yield where available and extrapolating the integral analytically to large m_t . The results are compared to the predictions of RQMD in Fig. 7. The shape of the rapidity distribution is rather well reproduced by RQMD over the entire range in rapidity covered by the present data. A similar agreement was also observed for the Si+A systems [22,23]. Small but significant deviations in the tail of the distribution are better visualized in the insets of the figure where the same distributions are shown on a logarithmic scale. In the range of our measurement the yields of both the positive and negative pions are systematically overpredicted by the RQMD 1.08 model with deviations that increase with rapidity and reaches a factor $\simeq 1.5$ at rapidity $y=4$.

C. π^-/π^+ ratio

Close inspection of the transverse mass curves of Fig. 6 reveals that the deviations from a pure exponential emission are systematically smaller for π^+ than for π^- . This charge asymmetry of the pion distributions is better studied by plotting the ratio of π^- to π^+ cross section as done in Fig. 8. In order to improve statistical errors on the ratio, the data were grouped into three larger rapidity bins. A strong charge asymmetry is observed starting at $m_t - m_\pi < 0.2 \text{ GeV}/c^2$ with a maximum value of $dN/dy(\pi^-)/dN/dy(\pi^+) \simeq 1.6$ at $m_t - m_\pi = 0 \text{ GeV}/c^2$ for the $y = 2.9 - 3.2$ rapidity slice. The measured asymmetry systematically decreases as a function of rapidity. The observed rapidity dependence is in agreement with the charge asymmetry measured by the E802 collaboration near y_{cm} for similar centrality [4].

The observed pion charge asymmetry and its rapidity dependence can be attributed to the different Coulomb potentials seen by the two type of pions at freeze-out. The Coulomb origin of this effect is supported by the results of the RQMD calculations which do not take into account final state interaction of the reaction products (second row of Fig. 8). As

expected, RQMD predicts no significant m_t dependence in the ratio of the pion cross section with an overall excess of negative pions of $\approx 20\%$.

In heavy systems, anomalously large π^-/π^+ ratios have been attributed to the effect of Coulomb interaction over a wide range of beam energies [24–31]. At the AGS, the first evidence of Coulomb effects in heavy systems was reported in ^{28}Si induced reactions [32,33].

We have used a simple model to study if the measured rapidity and m_t dependence of the π^-/π^+ ratio can be explained by the Coulomb interaction. The model is built along the line of the argument presented in [34,35] and similar to that discussed in [31]. It uses an effective central Coulomb potential to simplify the difficult many-body problem.

Assuming that the *fireball* is at rest in the center-of-mass and neglecting its time evolution, the effective Coulomb potential V_C seen by a singly-charged test particle is given by,

$$V_C = \frac{Z_{\text{eff}} \cdot e^2}{r_i} \quad (1)$$

where the effective charge $Z_{\text{eff}} < Z_A + Z_B$ is expected to be smaller than the total charge present in $A + B$ collisions and r_i is the radius at which the particle leaves the fireball. After exiting from the Coulomb potential well, the measured energy $E(p)$ of a test particle of positive/negative charge becomes

$$E(p) = E(p_i) \pm V_C \quad (2)$$

where p_i are the initial momentum and position at freeze-out. The number of particles per unit of momentum is then expressed as

$$n(p) = n(p_i) \frac{d^3 p_i}{d^3 p} = \frac{p_i E(p_i)}{p E(p)} n(p_i) \quad (3)$$

where $n(p_i)$ is the initial particle distribution and $d^3 p_i/d^3 p$ is the Jacobian deduced from energy conservation [35]. The initial single particle distribution $n(p_i)$ is therefore changed in magnitude as well as distorted by the Coulomb field. The Coulomb field induced distortion \mathcal{C} , can then be written as :

$$C^\pm = \frac{p_i E(p_i)}{p E(p)} \quad (4)$$

$$= \sqrt{p^2 \mp 2E(p)V_C + V_C^2} \cdot \frac{(E(p) \mp V_C)}{p E(p)} \quad (5)$$

for positively/negatively charged particles. The Coulomb distortion of the pion ratio is expressed in terms of measured momenta p as

$$\frac{\pi^-}{\pi^+}(p) = R \cdot \frac{C^-}{C^+} \cdot \frac{n(p_i^-)}{n(p_i^+)} \quad (6)$$

$$= R \cdot \frac{\sqrt{p^2 + 2E(p)V_C + V_C^2}}{\sqrt{p^2 - 2E(p)V_C + V_C^2}} \cdot \frac{(E(p) + V_C)}{(E(p) - V_C)} \cdot \frac{n(p_i^-)}{n(p_i^+)} \quad (7)$$

where R is an overall normalization constant. The transverse momentum and rapidity dependences are introduced by substituting $E = m_t \cosh(y)$ and $p = \sqrt{E^2 - m^2}$. Thus, the model predicts the shape of the π^-/π^+ ratio as well as its rapidity dependence with only two free parameters: the effective Coulomb potential V_C and the normalization constant R .

The model neglects the deflection of the particle trajectories induced by the Coulomb interaction. It is assumed that the initial angle of the particle (p_t/p_z) is conserved. Possible quantum mechanical effects are ignored and we also neglect the possible contribution from the spectators. Such a contribution has been discussed at lower energies [34,36]. However, our analysis concerns only the most central collisions where the fraction of the total charge carried by the spectators is relatively small. Also, the projectile spectators are far from the central fireball at $t \approx 9$ fm/c, the typical pion emission time determined by 2 particle correlation studies [39]. The model also assumes a static effective potential that is identical for all the particles. This approximation is not valid in general. However, here we discuss mainly high rapidity pions that are in the tail of the dN/dy rapidity distribution. Thus, on the average, these pions see a relatively similar central fireball at freeze out. This also justifies the neglect of the expansion of the fireball. These approximations are less valid as one approaches mid-rapidity.

The undistorted $n(p_i^\pm)$ distributions are not accessible experimentally. In the present calculation, in agreement with the RQMD prediction, we assume that both distributions

are similar in shape. The initial spectral shapes are generated using mean values of the parameters used in the two-exponential description of the data (see Fig. 6).

The model predictions are compared to the measured ratios of pion transverse mass spectra in Fig. 9. The predictions of the Coulomb distortion model (solid lines) are obtained from a fit to the first four measured distributions where the observed effect is the largest. The values of $V_C \approx 31 \pm 22$ MeV and $R \approx 0.92 \pm 0.14$ are found to best describe the shape and rapidity dependences of the pion ratio. These parameters are found to be still in agreement with the data at larger rapidities. The errors of the fitted values (dotted lines) are rather large, because there is a strong correlation between the effect of the relative normalization constant R and that of the effective Coulomb potential value.

The Coulomb induced distortion has two components: a Coulomb factor $\mathcal{C}^-/\mathcal{C}^+$ and an amplitude factor $n(p_i^-)/n(p_i^+)$ that is related to the shape of the initial pion spectra. The effects of R and V_C can not be distinguished above transverse mass values of about 0.25 GeV/ c^2 since the Coulomb distortion is rather flat and affects mainly the ratio of the pion yield. At low m_t , the two factors distort the shape of the pion ratio in a similar way, but quantitatively most of the distortion is attributable to the Coulomb factor.

Note, that secondary π^- from lambda decay will generate an excess of negative pions. This effect was studied by a Monte Carlo simulation using as input the lambda spectrum predicted by RQMD and taking into account the acceptance of the E877 spectrometer. This calculation shows that in the rapidity range discussed here the contribution from Λ decay is negligible above $m_t - m_{\pi^-} = 0.1$ GeV/ c^2 and contribute at most 10-15% of the observed asymmetry at $m_t - m_{\pi^-} = 0$, where this effect is maximum. We verified the influence of this uncertainty on the derived values of V_C by modifying the data set in agreement with the calculated influence of Λ decay. The effect on the results was found to be of the order of 2 MeV and thus negligible when compare to the large uncertainty originating from the strong correlation between V_C and R .

The present value of V_C is in a good agreement with the Coulomb potential obtained from a similar analysis of the pion spectra in Au+Au collisions at a bombarding energy of

1 GeV/nucleon [31].

The uncertainty on the value of the R and V_C constants could be improved with a larger data sample, *e.g.* by providing a measurement that would extend to larger values of m_t . Such data would better fix the relative values of R and V_C while the shape at low m_t would fix the magnitude of V_C . We remark also, that a more precise estimate of the effect of the Coulomb field on the measured pion spectra should take into account the effect of radial flow and emission time [37,38].

The pion rapidity distribution should also show effects of the Coulomb interaction since this interaction not only affects the transverse momentum but also the final rapidity of the emitted pions. We have shown in Fig. 7 that the π^+ and π^- have similar rapidity distributions reasonably well reproduced by RQMD with, however, increasing deviations at very forward rapidity. In Fig. 10, the ratio of the pion yield $dN/dy(\pi^-)/dN/dy(\pi^+)$ is plotted as a function of rapidity. One observes that the ratio shows a systematic decrease towards high rapidities while the RQMD 1.08 model (dashed histogram) predicts a very flat if anything slightly opposite rapidity dependence.

We have used the Coulomb distortion model developed here to determine if we can provide a consistent description of the effects observed both in the transverse mass spectra and in the rapidity dN/dy distribution. The dN/dy ratios calculated using the parameters $V_C = 31$ MeV and $R = 0.92$ deduced from the shape of the m_t spectra are shown by the solid line in Fig. 10. The calculated ratios are obtained by integrating the calculated distorted transverse mass distribution.

The rapidity dependence of the data is very well reproduced by the model over the entire measured rapidity range. The effective Coulomb field in Au+Au collisions is strong enough to significantly distort the rapidity distributions of light particles and, as shown in the figure, the ratio of pion dN/dy can vary by more than 20% depending on the rapidity at which it is measured. This result shows that light particle yield ratios should be interpreted with care and the comparison of yield ratios from experiments performed at different rapidities should take into account potential Coulomb effects.

It is interesting to compare the expected Coulomb potential viewed by the first pions that are ejected from the fireball to the effective Coulomb potential V_C obtained from our simple model. Using a simple geometrical model it is estimated that the mean total charge of the participants for the present event sample is $Z \approx 150$. Hanbury-Brown-Twiss (HBT) analysis of pion correlations provides an estimate of the fireball radius. One-dimensional HBT analysis of Au+Au central gives radius of ≈ 6.0 fm [40–43]. These numbers lead to uniformly-charged-sphere Coulomb potential values of $V \approx 36$ MeV, an estimate consistent with the value obtained from our simple model of the Coulomb interaction.

IV. CONCLUSIONS

In summary, we have presented new results on the spectra and multiplicity distributions of protons and pions emitted at forward rapidity in Au+Au collisions at 10.8A GeV/c. When combined with the data from E802 experiment [4] we now have a measurements of proton and pion production in central Au+Au collisions at AGS energy over the complete phase space.

The shape of the rapidity distribution of the protons over the entire range in rapidity covered by the present data, is rather well reproduced by RQMD 1.08 . The measured transverse momentum spectra have, however, larger inverse slope parameters than predicted by the model. This is consistent with the presence of a larger collective transverse flow than predicted by a pure cascade model.

The shape of the spectra and multiplicity distributions of the pions are very well described by RQMD. Systematic differences between the π^- and π^+ spectra at low values of the transverse momentum are, however, observed that are not predicted by the model. It is shown using a simple model that the observed effect is consistent with that expected from the different Coulomb potential felt by the two types of pions. Our simple analysis shows that the π^-/π^+ ratio provides an additional way, complementary to the Hanbury-Brown-Twiss interferometry and particle correlation analysis, for studying source sizes and dynamics.

ACKNOWLEDGMENTS

We wish to thank the Brookhaven Tandem and AGS staff for their excellent support and are particularly grateful for the expert help of W. McGahern and Dr. H. Brown. We also wish to acknowledge the important technical support provided by R. Hutter and J. Sondericker. Financial support by the US DoE, the NSF, the Canadian NSERC, and CNPq Brazil is acknowledged.

REFERENCES

- [1] J. Barrette *et al.*, the E814/E877 Collaboration, Phys. Rev. Lett. **70**, 2996 (1993).
- [2] J. Barrette *et al.*, the E877 Collaboration, Phys. Rev. **C 51**, 3309 (1995).
- [3] J. Stachel, Nucl. Phys. **A654**, 119 (1999); Proceedings of Int. Nucl. Phys. Conf. (INPC98), Paris, France, 24-28 August, 1998 ; nucl-ex/9903007
- [4] L. Ahle *et al.*, the E802 Collaboration, Phys. Rev. **C 57**, R466 (1998).
- [5] J. Barrette *et al.*, the E814 Collaboration, Phys. Rev. **C 50**, 3047 (1994).
- [6] R. Lacasse *et al.*, Nucl. Instr. Meth. in Phys. Res. **408**, 408 (1998).
- [7] R. Lacasse, Ph.D. thesis, McGill University, 1998.
- [8] T. W. Piazza, Ph.D. thesis, SUNY at Stony Brook, 1997.
- [9] S. Voloshin, E877 note HD-96/08/15 .
- [10] R. Brun *et al.*, Geant 3 Users Guide, CERN Data Handling Division Report No. DD/EE/84-1, 1984.
- [11] J. Barrette *et al.*, the E814 Collaboration, Phys. Rev. **C 45**, 819 (1992).
- [12] H. Sorge, H. Stöcker, W. Greiner, Ann. Phys. (N.Y.) **192**, 266 (1989).
- [13] T. Abbott *et al.*, the E802 Collaboration, Phys. Rev. **C 50**, 1024 (1994).
- [14] P. Braun Munzinger, J. Stachel, J. P. Wessels, Xu Nu, Phys. Lett. **B344**, 43 (1995).
- [15] R. Mattiello, A. Jahns, H. Sorge, H. Stöcker, and W. Greiner, Phys. Rev. Lett. **74**, 2180 (1995).
- [16] P. Braun Munzinger, J. Stachel, J. P. Wessels, Xu Nu, Phys. Lett. **B365**, 1 (1996).
- [17] J. Barrette *et al.*, the E877 Collaboration, Phys. Rev. **C 56**, 3254 (1997).
- [18] J. Barrette *et al.*, the E814 Collaboration, Phys. Lett. **B351**, 93 (1995).

- [19] G.E. Brown, J. Stachel, and G.M. Welke, Phys. Lett. **B253**, 19 (1991).
- [20] B.-A. Li, Phys. Letts. **B254**, 335 (1991).
- [21] J. Sollfrank, P. Koch, and U. Heinz, Phys. Letts. **B252**, 256 (1990).
- [22] T.K. Hemmick for the E814 Collaboration, Nucl. Phys. **A566**, 435c (1994).
- [23] M. Gonin, Ole Hansen, R. Moskowitz, F. Videbæk, H. Sorge, R. Matiello, Phys. Rev. **C 51**, 310 (1995).
- [24] W. Beneson *et al.*, Phys. Rev. Lett. **43**, 683 (1979).
- [25] G. Bertsch, Nature **283**, 280 (1980).
- [26] K. L. Wolf *et al.*, Phys. Rev. Lett. **42**, 1448 (1979).
- [27] S. Nagamiya *et al.*, Phys. Rev. **C 24**, 971 (1981).
- [28] K. L. Wolf *et al.*, Phys. Rev. **C 26**, 2572 (1982).
- [29] B.-A. Li, Phys. Lett. **B346**, 5 (1995).
- [30] H. Bøeggild *et al.*, Phys. Lett. **B372**, 339 (1996).
- [31] A. Wagner *et al.*, Phys. Lett. **B420**, 20 (1998).
- [32] M. Gonin for the E802/E866 Collaboration, Nucl. Phys. **A566**, 601c (1994).
- [33] F. Videbæk for the E802 Collaboration, Nucl. Phys. **A590**, 249c (1995).
- [34] M. Gyulassy and S. K. Kauffmann, Nucl. Phys. **A362**, 503 (1981).
- [35] G. Baym and P. Braun-Munzinger, Nucl. Phys. **A610**, 286c (1996).
- [36] K. G. Libbrecht and S. E. Koonin, Phys. Rev. Lett. **43**, 1581 (1979).
- [37] M. G.-H. Mostafa and C.-Y. Wong, Phys. Rev. **C 51**, 2135 (1995).
- [38] H. W. Barz, J. P. Bondorff, J. J. Gaardhøeje, and H. Heiselberg, Phys. Rev. **C 56**, 1553

(1997).

- [39] J. Barrette *et al.*, the E814 Collaboration, Phys. Lett. **B333**, 33 (1994).
- [40] J. Barrette *et al.*, the E877 Collaboration, Phys. Rev. Lett. **78**, 2916 (1997).
- [41] D. Miśkowiec for the E877 Collaboration, Nucl. Phys. **A610**, 227c (1996).
- [42] M. D. Baker for the E859/E866 Collaboration, in *HIPAGS '96* (Wayne State University, Detroit, 1996), pp. 159–165.
- [43] M. D. Baker for the E802 Collaboration, Nucl. Phys. **A610**, 213c (1996).

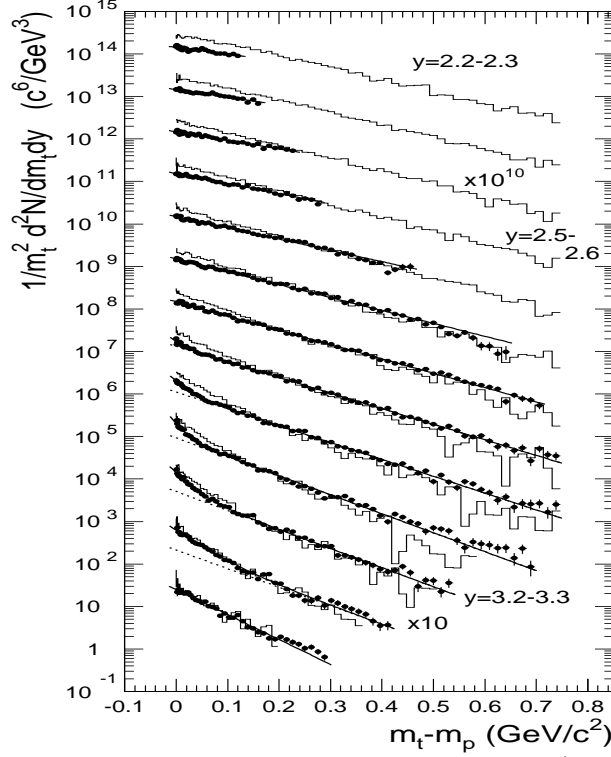


FIG. 1. Transverse mass spectra for protons produced in central ($\sigma_{central}/\sigma_{geom}=0.04$) Au+Au collisions. The dots correspond to constant p_t bins of 20 MeV, and y bins of 0.1 units. Beginning with rapidity bin $y=3.3-3.4$, spectra have been multiplied by successively increasing factors of ten. Full lines are two component exponential fits to the data. The histograms are RQMD predictions.

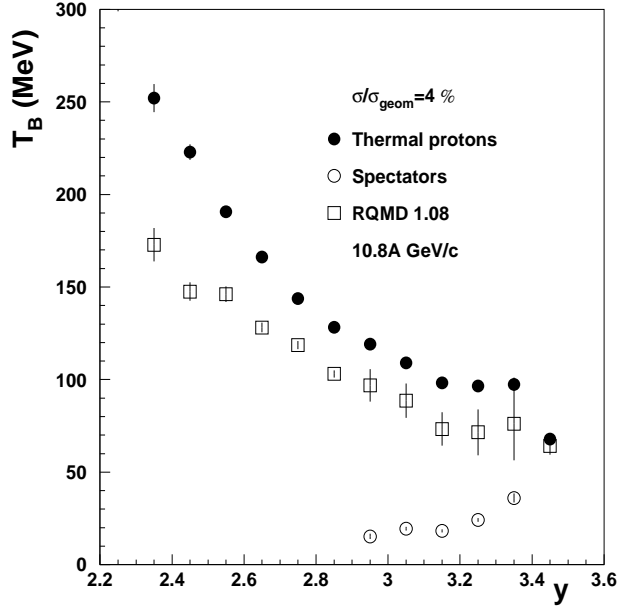


FIG. 2. Inverse slope parameters deduced from fits to the proton m_t spectra for central Au+Au collisions. The solid circles correspond to the high m_t component and the open circles correspond to the low m_t component. The squares are the results for the high m_t component of a similar fit to the calculated spectra.

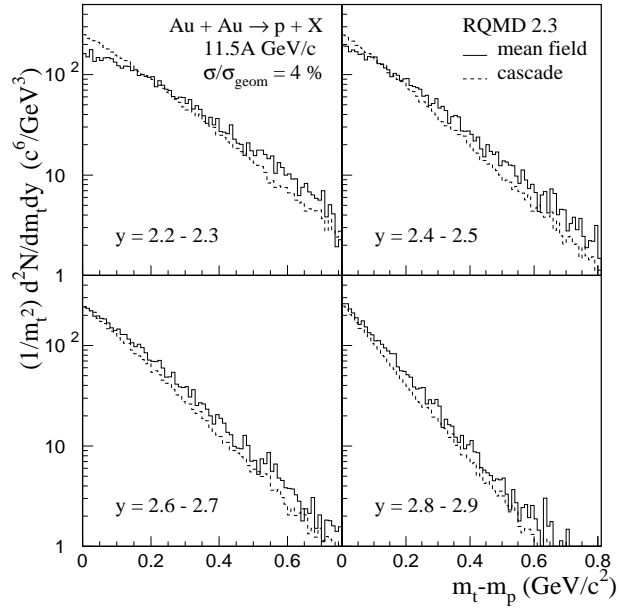


FIG. 3. Comparison of the proton transverse mass spectra for central Au+Au collisions at 11.5A GeV/c predicted by RQMD 2.3 run in a cascade mode (dashed histograms) and including the effects of mean field (full histograms).

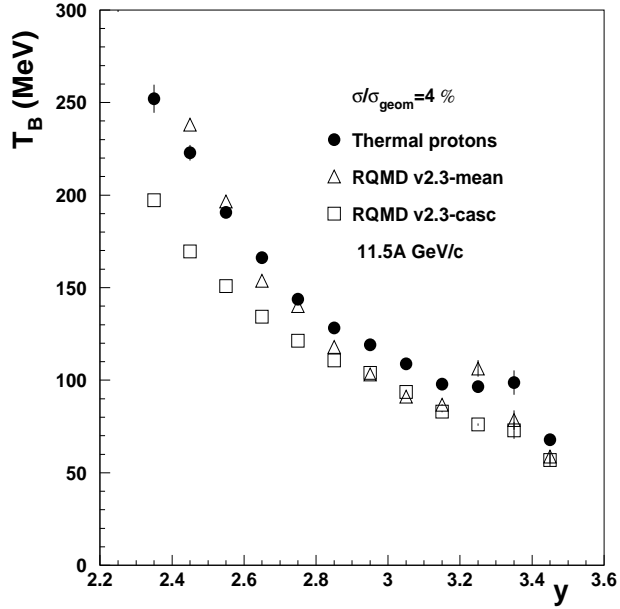


FIG. 4. Inverse slope parameters deduced from fits to the proton m_t spectra for central Au+Au collisions. The solid circles correspond to fits to the high m_t component of the experimental spectra at 10.8 GeV/c. The open symbols are the results of a similar fit to the calculated spectra at 11.5 GeV/c predicted by RQMD 2.3 - in cascade mode (squares) and with mean field included (triangles).

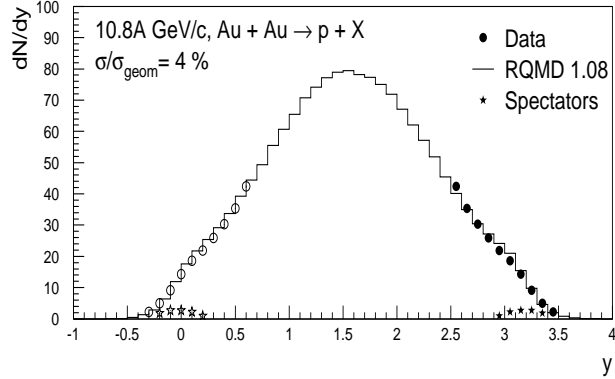


FIG. 5. Rapidity distributions for protons in central Au+Au collisions. Filled symbols represent measured data, open symbols reflected data. The stars correspond to the contribution from the low m_t component to the total measured multiplicity (circles). The histogram shows the results from RQMD calculations.

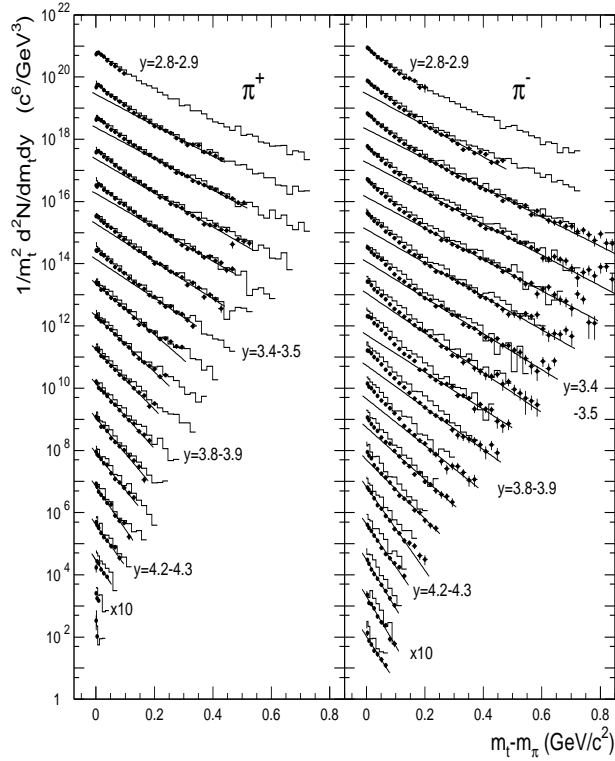


FIG. 6. Pion transverse mass spectra for central ($\sigma_{central}/\sigma_{geom}=0.04$) Au+Au collisions. Beginning with $y=4.4-4.5$, the spectra have been multiplied by successively increasing factors of ten. Full lines are the results of Boltzmann fits to the data over a limited range (see text). The histograms are RQMD predictions.

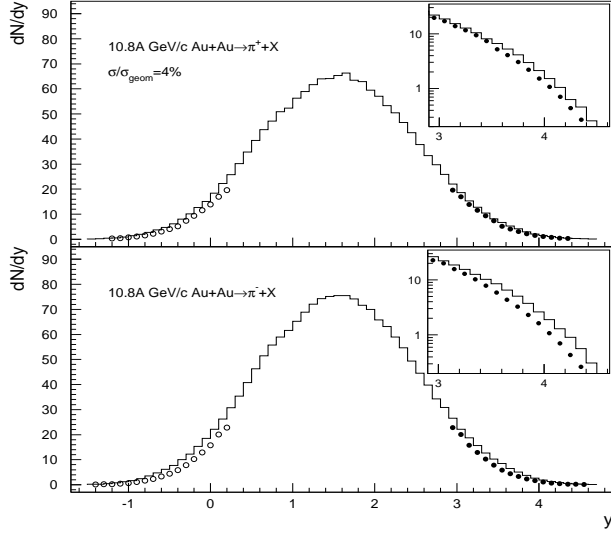


FIG. 7. Rapidity distributions for charged pions (dots) in central Au+Au collisions. Measurements are reflected (open symbols) about mid rapidity. Also shown are the results from RQMD calculations (histogram). The insets show the high rapidity part of the distributions on a logarithmic scale.

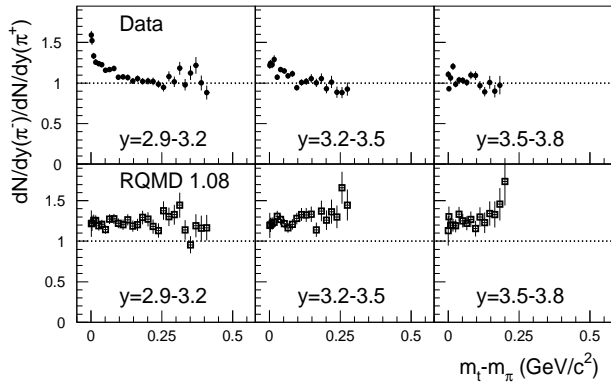


FIG. 8. Top row; transverse mass dependence of the experimental pion cross section ratio π^-/π^+ for three rapidity intervals. Bottom row; corresponding RQMD predictions for the π^-/π^+ cross section ratio.

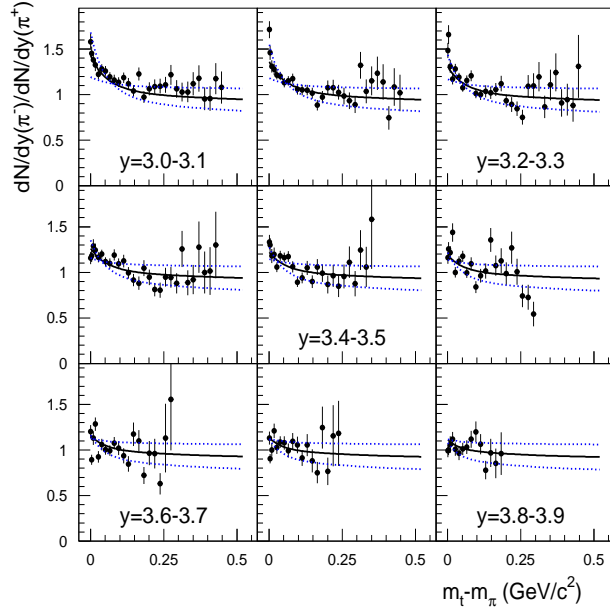


FIG. 9. The π^-/π^+ ratio as a function of transverse mass for nine rapidity intervals. The solid line is the result from a Coulomb distortion calculation. The dotted lines show the statistical error of the fit.

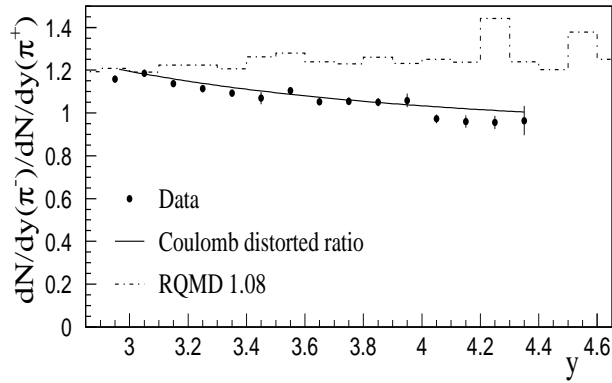


FIG. 10. Rapidity distribution of the experimental π^-/π^+ cross section ratio (dots). Also shown are the calculated ratio taking into account the effect of Coulomb distortion (full line) and the results from RQMD calculations (histogram).